Medium-scale resonant wave barrier for seismic surface waves

Medium-scale resonant wave barrier for seismic surface waves

Farhad Zeighami[a], Antonio Palermo[a], Athanasios Vratsikidis[b], Zhibao Cheng[c], Dimitris Pitilakis[b], Alessandro Marzani[a,*]

[a] *University of Bologna, Department of Civil, Chemical, Environmental and Materials Engineering - DICAM, 40136, Bologna, Italy.*

[b] *Aristotle University of Thessaloniki, 424 GR-54124 Thessaloniki, Greece.*

[c] *Beijing Jiaotong University, Beijing, 100044, China.*

Words counts: 6297

Characters count (with spaces): 41130

Characters count (not including spaces): 34892

* Corresponding Author: Alessandro Marzani. Email: alessandro.marzani@unibo.it

Medium-scale resonant wave barrier for seismic surface waves

ABSTRACT

The emergence of seismic metamaterials has led to the development of several novel isolation devices viable for seismic and ground-borne vibration control. Locally resonant barriers, also known as metabarriers, are one of those devices made of a cluster of near-surface resonators. The resonant frequency of these meter-size mechanical resonators is tuned to fall within the frequency spectrum of seismic surface waves. Resonant wave barriers can be placed around the critical structures or infrastructures to attenuate the Rayleigh induced ground motions and mitigate the risk of seismic hazards. Although the vibration attenuation capabilities of the resonant wave barriers are validated by numerical simulations and a few table-top experiments, their full-scale experimental validation is still unexplored. In this work, we design an experimental campaign, to be carried out in the Euroseistest site (Mygdonia, Greece), to assess the attenuation performance of a medium-size scale resonant wave barrier operating within the frequency range of 50−100 Hz. Soil properties are considered to develop the numerical simulations aimed at designing of the metabarrier and the on-field experimental test. In particular, the dispersive properties of (i) bare soil, (ii) a configuration of "dead masses" placed over the soil surface, and (iii) a metabarrier, are compared numerically. The resonant barrier introduces a significant amplitude reduction of the surface waves in a narrow frequency range around the resonant frequency of the resonators. Multiple-frequency barriers are designed with increasing and decreasing resonant frequencies to enlarge the attenuation frequency band. This variable-frequency design approach is obtained by tuning the mass or stiffness of the resonators. We expect that the medium-scale experimental tests, designed according to the presented numerical framework, will confirm the attenuation of the ground motion in the presence of the resonant wave barrier.

Seismic Metamaterials; Surface waves; Ground vibration mitigation; Dispersion analysis; Metabarrier.

1. Introduction

Since their emergence in electromagnetism (Pendry, Holden, Stewart, & Youngs, 1996), metamaterials have been translated into several domains, including the elastodynamics, and have found applications in civil engineering. In this latter context, metamaterial-based devices are proposed as an alternative solution to the existing seismic isolation methods (Furinghetti & Pavese, 2017; Mazza & Sisinno, 2017) to mitigate the effects of seismic waves and thus protect historical sites, urban areas, as well as vulnerable structures and infrastructures (Antoniadis, Kanarachos, Gryllias, & Sapountzakis, 2018; Bao, Shi, & Xiang, 2011; Basone, Wenzel, Bursi, & Fossetti, 2019; Cheng & Shi, 2018; Krödel, Thomé, & Daraio, 2015; Miniaci, Krushynska, Bosia, & Pugno, 2016; Palermo, Krödel, Marzani, & Daraio, 2016; Palermo et al., 2019; Pu & Shi, 2018; Shi, Cheng, & Xiang, 2014). This class of devices, frequently indicated as "seismic metamaterials" from the seminal work by Brûlé et al. (Brûlé, Javelaud, Enoch, & Guenneau, 2014), includes periodic and resonant foundations as well as periodic and resonant wave barriers able to interact with the propagation of seismic waves.

The use of periodic structures finds its inspiration on the dynamic behaviors of phononic crystals, periodic artificial composites characterized by large spectral frequency bandgaps (Kadic, Bückmann, Schittny, & Wegener, 2013). In these frequency regions, the propagation of waves with wavelengths in the order of material periodicity is inhibited (P. A. Deymier, 2013). In the context of ground motion attenuation, phononic crystals constituted by meter-size holes drilled in a periodic arrangement along the soil surface have been experimentally tested to attenuate the

propagation of soil vibration at frequencies around 50 Hz (Brûlé et al., 2014). Similarly, a periodic arrangement of concrete columns with variable dimensions has been proposed to modify the velocity of propagation of seismic waves and reroute them around a protected area (Colombi, Guenneau, Roux, & Craster, 2016), exploiting concepts of ray theory and lens designing. Additionally, a periodic arrangement of rigid columns embedded in soft and thin sedimentary basin overlaying the bedrock is another example of phononic-based seismic metamaterials designed to prove the opening of a broadband zero-frequency bandgap (Achaoui et al., 2017).

In general, since seismic waves are characterized by long wavelengths, phononic based devices result in large meta-structures, of questionable practical implementation for low-frequency ground vibrations (< 30 Hz). For this reason, locally resonant metamaterials have been proposed to construct seismic isolation devices with dimensions independent from the wavelength of the incoming seismic wave. In fact, resonant metamaterials exploit arrays of resonant units able to interact with seismic waves at a sub-wavelength scale. This approach has led to the development of the so-called metafoundations and metabarriers. Resonant metafoundations consist in an array of mass-spring systems embedded in the foundations to isolate the related upper structure (Cheng & Shi, 2013; Cheng et al., 2020; Sun, Xiao, & Bursi, 2020; Yan et al., 2014). Metabarriers, instead, consists of an array of locally resonant units embedded close to the soil surface, capable of shielding buildings and infrastructures from surface Rayleigh (Dertimanis, Antoniadis, & Chatzi, 2016; Palermo et al., 2016) or Love waves (Maurel, Marigo, Pham, & Guenneau, 2018).

The resonant units, placed at a subwavelength distance and tailored to operate in the low-frequency range of the seismic action, are capable of converting surface Rayleigh waves into bulk shear waves. Nonetheless, the possibility of achieving a low-frequency range of attenuation is counteracted by the narrow frequency operation of these devices, which can be significantly enlarged only by means of large resonant masses or units with varying resonant frequencies (Colombi, Colquitt, Roux, Guenneau, & Craster, 2016). The trade-off between the amount/number of resonant mass and the attenuation efficiency of these devices, together with concerns about the physical implementation and structural integrity of these systems, are open issues that require an in-depth investigation supported by experimental evidence. Indeed, although the dynamics of the resonant wave barriers are well-described by analytical models (Colquitt, Colombi, Craster, Roux, & Guenneau, 2017; Maurel et al., 2018), and numerical simulations (Palermo et al., 2016), experimental validations of these devices are still limited to few small-scale experiments for surface Rayleigh (Palermo et al., 2018), and shear waves (Zaccherini et al., 2020). At the geophysical scale, the coupling between surface waves and distributed resonators has been evinced only by analysing the propagation of ground vibrations through forest trees (Colombi, Roux, Guenneau, Gueguen, & Craster, 2016). However, an investigation on the behavior of true-scale barriers for seismic surface wave mitigation would require a high cost of realization due to the soil excavation works and resonant unit manufacturing, suggesting first the design of a medium-scale experimental campaign, able to test the dynamics of such resonators on the field.

In what follows, we present the numerical design of an experimental campaign aimed

at assessing the attenuation performance of a medium-scale wave barrier within the frequency range of 50 − 100 Hz. The experimental campaign is set to be run in the Euroseistest facility, where the characteristics and dynamic properties of the soil are well-known (D. Pitilakis, Dietz, Wood, Clouteau, & Modaressi, 2008).

The experimental campaign aims to test and confirm the expected attenuation capability of the resonant wave barrier for the surface ground motion, taking into account the in-situ soil properties of the Euroseistest facility (http://euroseisdb .civil.auth.gr), and the operating frequency range of the source and the measuring instruments. The paper is organized as follows. In Sec.2, we will provide the soil properties of the test site and describe the components and arrangement of the designed wave barrier. In Sec. 3, we test the performance of the barrier through a numerical dispersion analysis and provide numerical predictions via time transient simulations. We design frequency-variable resonant barriers and compare their seismic isolation performance with those of a single-frequency barrier in Sec 4. Finally, some conclusions are drawn in Sec.5.

2. A medium-scale resonant wave barrier

2.1.Site Description

As the mechanical properties of the soil can remarkably influence the frequency spectra and amplitude decay of surface waves propagating across a resonant wave barrier (Palermo et al., 2018), it is essential to know the characteristics of each soil stratum to design the wave barrier properly.

Euroseistest is a geotechnical test site located in the center of a tectonically active graben of Mygdonia, about 30 km to the NE of the city of Thessaloniki in northern Greece (K. Pitilakis, Raptakis, Lontzetidis, Tika-Vassilikou, & Jongmans, 1999). The site was the epicenter of the 1978 Thessaloniki earthquake with a magnitude of 6.5 M_w. The soil stratification, mechanical and dynamic properties of the Mygdonia basin have been carefully evaluated through extensive seismic - geophysical campaigns, in-situ geotechnical surveys, and laboratory testing (D. Pitilakis et al., 2008; D. Pitilakis, Rovithis, Anastasiadis, Vratsikidis, & Manakou, 2018; K. Pitilakis et al., 1999; Raptakis, Chavez-Gracia, Makra, & Pitilakis, 2000). The well-documented depth-dependent longitudinal and shear bulk wave speeds and density of the soil (ρ = 1500 kg/m3) allows for a proper design of the metabarrier (see Fig. 1).

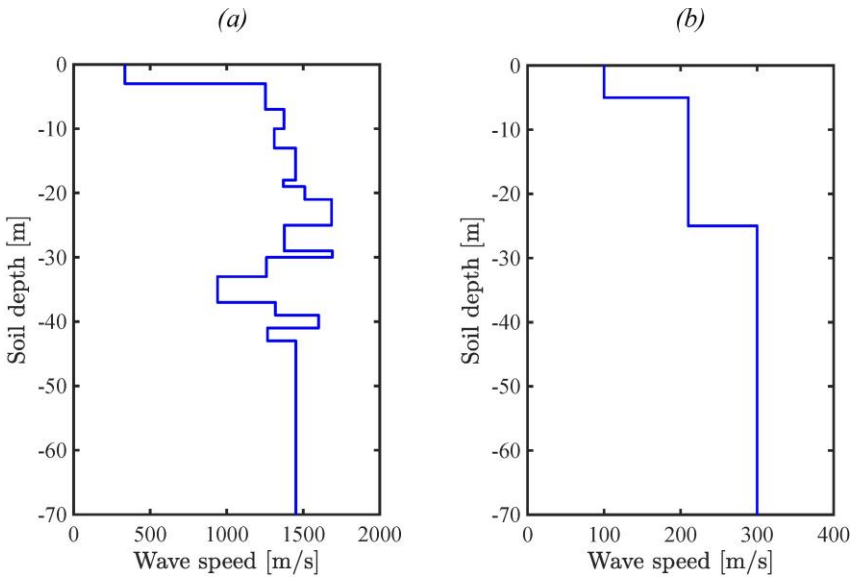

Figure 1. (a) Longitudinal and (b) shear waves speed profiles of the Euroseistest site (D. Pitilakis et al., 2018).

2.2.The Resonant Barrier

We study a barrier of resonators, dubbed as metabarrier, consisting of an array of 5 ×

10 surface resonators arranged in a regular square grid with a spacing of 0.7 m (see the top view in Fig. 2a). These dimensions are sufficiently small to guarantee that resonators interact at a sub-wavelength scale. Similar configurations have been numerically studied to assess the attenuation of seismic surface waves exploiting the horizontal (Krödel et al., 2015) and vertical (Palermo et al., 2016) vibration modes of the resonators. Here, we focus our study on the coupling of surface waves with the vertical resonances f_r of each resonator. We design simple and cost-effective resonators using steel springs and PVC barrels filled with sand, as shown in Fig. 2b. The prototype resonator consists of a 60 liter PVC barrel (diameter 40 cm and height approximately 50 cm), two steel plates (40×40×1 cm) suspended by 4 to 8 vertical steel springs. The base plate is anchored to the soil surface via four steel bolts. The barrels are filled with dry sand, for a total mass of 100 kg. Besides, a twin configuration realized only with barrels, e.g., without steel plates and springs to connect the barrels to the ground, is designed to mimic the effect of an array of "dead masses", as shown in Fig. 2c.

The resonant frequency of the resonator is tailored to provide a surface wave attenuation between 45 and 50 Hz, well above the seismic frequency range (< 10 Hz). By varying the number of springs and filling volume of the sand, we can alter the overall stiffness and mass of the resonators, to obtain a modular and flexible design of the metabarrier during experiments. For instance, for a mass of 100 kg and a resonant frequency f_r = 50 Hz, the overall springs stiffness is $K_{tot} = 100 \cdot (2\pi f_r)^2 = 9869.6\ kN/m$. In particular, the proposed design approach allows building an array of the graded resonators with variable (e.g., increasing or decreasing resonant)

frequencies, widening the attenuation frequency range of the barrier.

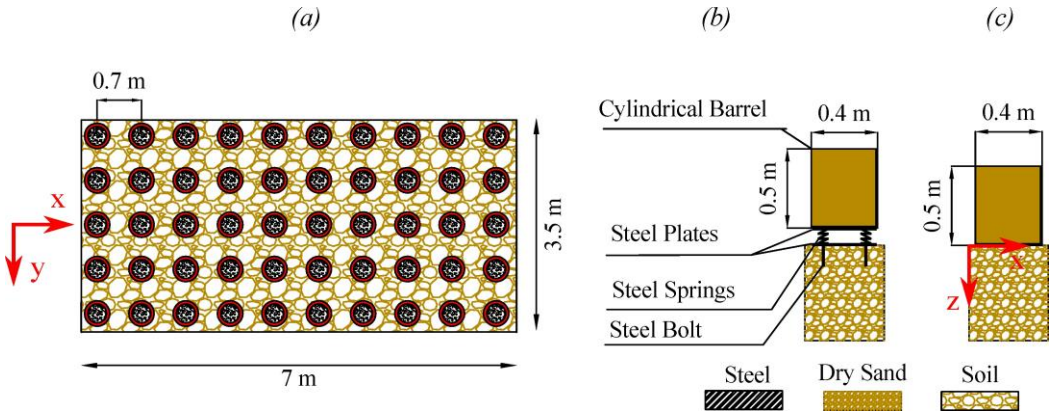

Figure 2. (a) Array of 5 × 10 resonators constituting the metabarrier (top view). (b) Schematics of a single resonator. (c) Schematics of a dead mass over the soil surface.

3. Numerical analysis of the resonant barrier

In this section, we develop Finite Element (FE) models to mimic and predict the performance of the designed metabarrier. First, we extract the dispersion of surface waves traveling through the barrier following the Wave Finite Element Model (WFEM) approach (Mace & Manconi, 2008). Then, we build full-scale FE models in accordance with the dispersion curves and evaluate the attenuation performance of the barrier. The validity of the presented numerical approach has been tested in our previous studies (Palermo et al., 2016, 2019).

3.1.Dispersion Analysis

We build 2D unit cell models under plane-strain conditions in Comsol Multiphysics to describe the dynamics of surface waves propagating through the wave barrier. We analyse the dispersive properties of three configurations: a portion of bare soil, labelled as the reference soil model (RSM), a portion of soil with a dead mass on top

(DM), and a unit cell of the resonant metabarrier (MB), e.g., a portion of the soil with the resonator on top. For the bare soil, we consider a column with a height of h = 70 m, and the length of w = 0.7 m, as shown in Fig. 3a. The depth-dependent speed profiles of the soil presented in Fig. 1 are assigned to the model. The unit cell domain is discretized by quadratic quadrilateral elements with a maximum dimension of d_{max} = 0.7 m. Bloch-Floquet conditions are applied to the lateral edges of the model to obtain the surface modes of the soil column. The dispersive properties (frequency vs. wavenumber) of the lowest four surface modes in the frequency range of 10 − 70 Hz are shown in Fig. 3b, together with the related phase velocities reported in Fig. 3c. As expected, multiple surface modes (e.g., $M1$-$M4$) are found due to the heterogeneity of the soil profile. An approximated prediction of the fundamental surface mode in the considered stratified soil is provided by employing a classical Rayleigh wave dispersion law for a homogeneous half-space (K.F. Graff, 1975):

$$\left(2-\left(\frac{\omega}{kc_S}\right)^2\right)^2-4\sqrt{1-\left(\frac{\omega}{kc_P}\right)^2}\sqrt{1-\left(\frac{\omega}{kc_S}\right)^2}=0 \qquad (1)$$

where, ω is the angular frequency, k is the wavenumber, c_P, and c_S are the longitudinal and transverse wave speed of upper layer of the stratified soil with $5m$ of depth, respectively.

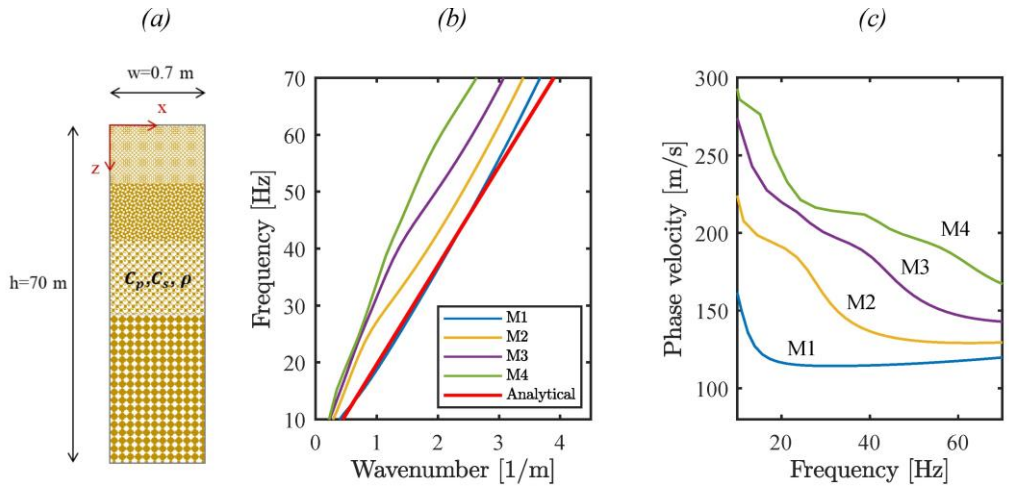

Figure 3. (a) Reference soil model (RSM) unit cell. Dispersion curves in terms of (b) frequency vs. wavenumber, and (c) phase velocity vs. frequency. Analytical prediction of the fundamental mode according to Eq. (1) (red line) is superimposed to the dispersion curves.

The dead mass (DM) configuration model is developed considering a unit cell of unitary thickness t = 1m and introducing an equivalent 2D mass per unit cell, to correctly model the total inertia of the dead mass in its 3D configuration (see Fig.4a). The surface wave dispersion curves of the DM configuration are displayed in Fig.4b. The presence of the mass slightly decreases the velocity of the surface modes in the high-frequency range (> 60 Hz).

The dispersion properties of the fundamental Rayleigh mode can be approximated analytically via Eq. (2), where the classical Rayleigh wave dispersion relation for a homogeneous half-space is modified by considering the effect of the dead masses via their inertia force at the free surface (Zeighami, Palermo, & Marzani, 2019) as:

$$\left(2-\left(\frac{\omega}{kc_S}\right)^2\right)^2-4\sqrt{1-\left(\frac{\omega}{kc_P}\right)^2}\sqrt{1-\left(\frac{\omega}{kc_S}\right)^2}=\frac{-M\omega^4}{S\rho {c_S}^4k^3}\sqrt{1-\left(\frac{\omega}{kc_P}\right)^2} \quad (2)$$

In Eq. (2), ρ is the density of the soil, $S = w \times t$ is the influence area of the dead mass, M is the mass of the DM, c_P, and c_S are the longitudinal and transverse wave speed of the lowest-order mode of the bare soil at f = 44 Hz (see Fig.3c), respectively. The analytical dispersion curve of Eq. (2) is superimposed to the numerical solutions as a continuous red line in Fig. 4b. It is evident that the analytical prediction of the homogeneous soil captures just the first mode of the stratified soil, suggesting the use of numerical models to better describe the dynamics of DM over the heterogeneous soil.

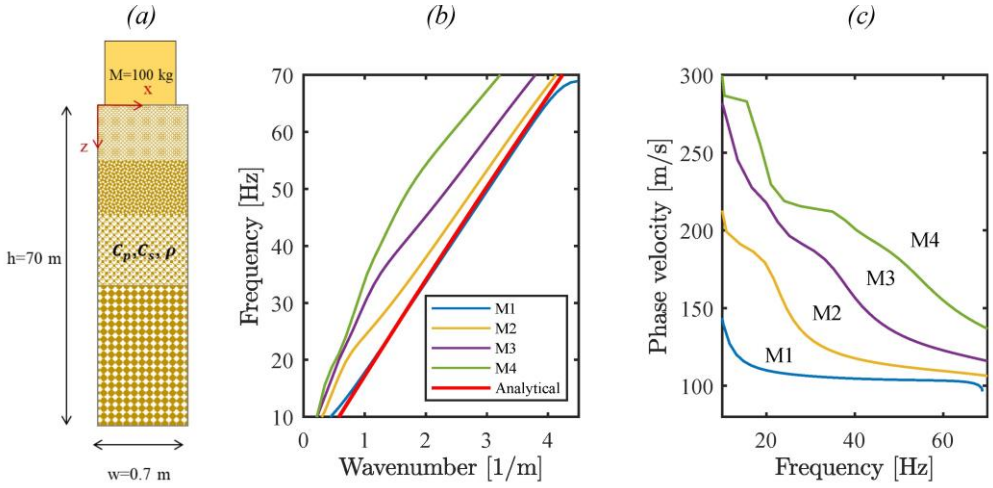

Figure 4. (a) Dead Mass (DM) unit cell. Dispersion curves in terms of (b) frequency vs. wavenumber, and (c) phase velocity vs. frequency. The superimposed red curve in the panel (b) has been obtained using Eq. (2).

We model the resonant barrier unit cell by placing two springs, each having vertical stiffness of $K_s = K_{tot}/2$, between the soil and the mass of the DM model (see Fig. 5a). The dispersive properties of surface waves interacting with the resonant barrier are

extracted from eigenfrequency analysis and plotted in Fig. 5b. The presence of the resonator in this dynamic system introduces a flat dispersive branch around 44 Hz, corresponding to the vertical motion of the resonator. The soil layer below the resonator acts as a soft spring, leading to the reduction of the nominal resonant frequency of the system, namely at 50 Hz. Similar to what is done for the DM case, we compare the numerical predictions with an analytical estimation of the Rayleigh fundamental mode interacting with the barrier via Eq. (3) (Palermo et al., 2016). The analytical expression accounts for the interaction between the resonant barrier dynamics and Rayleigh waves propagating in an idealized homogeneous and isotropic soil considering the longitudinal and transverse wave speeds obtained from the phase velocity of the lowest-order mode of the bare soil (see Fig.3c) at $f = 44$ Hz:

$$\left(\left(\frac{\omega}{\omega_r}\right)^2 - 1\right)\left[\left(2 - \left(\frac{\omega}{kc_S}\right)^2\right)^2 - 4\sqrt{1 - \left(\frac{\omega}{kc_P}\right)^2}\sqrt{1 - \left(\frac{\omega}{kc_S}\right)^2}\right] = \frac{M\omega^4}{S\rho {c_S}^4 k^3}\sqrt{1 - \left(\frac{\omega}{kc_P}\right)^2} \tag{3}$$

In Eq. (3), $\omega_r = 2\pi f_r$ is the natural frequency, and $S = 0.7m^2$ is the influence area of resonators.

The solution of such an analytical formulation superimposed to the numerical solutions as red lines in Fig. 5b, predicts for the homogeneous soil the existence of a surface wave bandgap (box in grey in Fig. 5b), enclosed within a flat dispersive branch (bottom edge) and the intersection of the surface mode with the bulk shear wave speed (upper edge). Within this frequency range, the propagation of Rayleigh waves is inhibited, and surface wave energy trajectory diverges from the surface to the soil bulk in the form of shear waves (Colombi, Roux, et al., 2016; Palermo et al.,

2016). Such a phenomenon is not observed in the case of stratified soils, as evident from Fig. 5b, where the bandgap region of the homogeneous soil is crossed by the higher-order surface modes (Palermo et al., 2018). However, also for a heterogeneous soil profile, the presence of the resonators induces the generation of a flat branch around the natural frequency of resonators $f_r = 44\ Hz$. Around this frequency, a strong wave attenuation is expected due to the impedance mismatch at the interface between the bare soil and soil equipped with resonators.

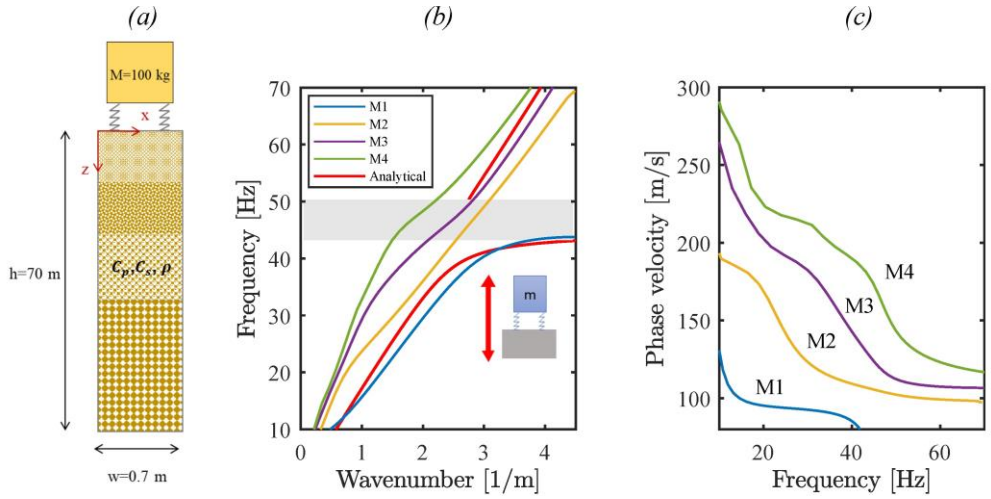

Figure 5. (a) Metabarrier (MB) unit cell. Dispersion curves in terms of (b) frequency vs. wavenumber, and (c) phase velocity vs. frequency. The curves reported as red lines in panel (b) have been obtained by Eq. (3).

Besides the dispersive properties, we also investigate the vertical mode profile of the soil column extracted from Bloch-FE dispersion relations at the resonance ($f_r = 44\ Hz$) comparing the DM and MB cases with the bare soil condition, e.g., RSM. The vertical displacements of 701 points equally distributed along the depth of the soil column with a spacing of 0.1 m are extracted. The results are normalized by the

maximum vertical nodal displacement of the corresponding mode and plotted versus the depth in Fig. 6 for $M1$, $M2$, $M3$, and $M4$ surface modes. We observe that the addition of dead masses to the soil surface does not substantially modify the soil displacement (see solid lines with asterisk marker in panel a of Fig. 6). Conversely, the presence of the resonator significantly changes the vertical displacement of the soil. In particular, the fundamental mode gets confined to the surface due to the coupling with the resonators, while all the higher-order modes assume almost vanishing displacement amplitude at the surface level $z = 0$ (see continuous lines in Fig. 6b). Hence, we expect that these modes do not contribute to the surface wavefield for the frequencies around the natural frequency of the resonator.

In the next section (Sec.3.2), time history analyses are performed to confirm the predictions of the dispersion analyses and to quantify the attenuation of surface waves for RSM, DM, and MB configurations.

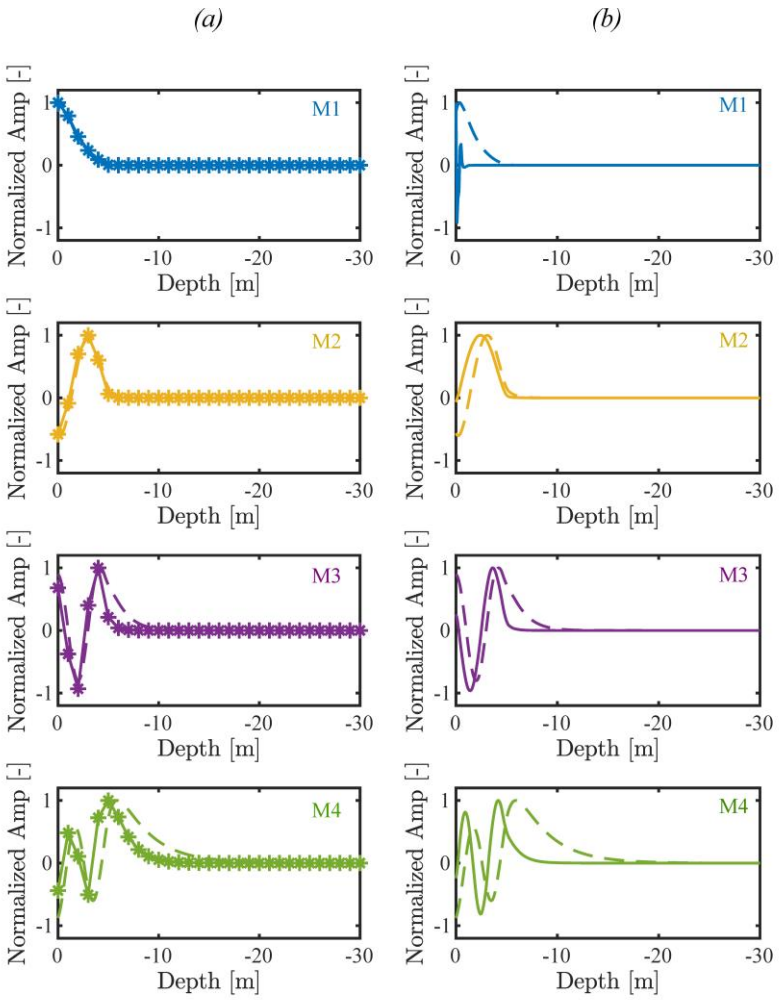

Figure 6. Normalized amplitude obtained from vertical nodal displacement for the dead mass (panel a) and metabarrier (panel b) cases vs. the RSM (dashed lines) at the resonant frequency of resonators (f_r = 44 *Hz*). In the presence of metabarrier, all the surface modes are characterized by a vanishing displacement at the soil surface (continuous lines in panel (b)).

3.2.Time History Analysis

Two-dimensional FE models are developed to mimic the open field experimental setup, and time transient simulations are performed to validate the numerical observations of the dispersion analyses. Three numerical models are compared: the

reference soil model (RSM), the case with an array of masses place over the soil without elastic connectors (DM), and the metabarrier (MB). A 2D domain with a dimension of 30 m × 70 m (see the model schematics in Fig. 7a) under plane-strain assumptions, is used to model the propagation of a surface wave travelling through an array of dead mass and resonators. The bottom corners of the model are constrained to prevent any unwanted rigid motion. In addition, Low Reflective Boundary Conditions (LRBCs) are applied to the lateral and bottom boundaries of the model to minimize wave reflections. LRBC uses the material properties of the adjacent media to create an impedance matched interface for the propagating longitudinal and shear waves. Soil density (ρ = 1500 kg/m^3) and depth-dependent speed profiles of Fig. 1 are assigned to the model. The field domain is discretized by quadratic quadrilateral elements with a maximum dimension of d_{max} = 0.7 m, identical to the unit cell models developed in Sec. 3.1.

Fig. 7b depicts the layout of the simulated experimental setup, where the positions of the wave source, resonators, and measuring instrumentation are reported. Eighteen geophones are used for the data acquisition, half of them (geophones A to I) measure the soil response along the barrier, namely output 1, and the rest (geophones J to R) measure the soil response after the barrier, namely output 2. A Ricker wavelet centered at the frequency of 50 Hz, able to sufficiently excite the whole frequency range of interest (0 − 100 Hz), generates surface waves from the source location, with an offset of 5 m from the edge of the model. The output wavefield is evaluated as the averaged vertical nodal displacement extracted over an array of 9 points with an overall length of 6.3 m (i.e., equivalent to the array of geophones in the design of

experiments) distributed along (e.g., output 1) and after the barrier (e.g., output 2).

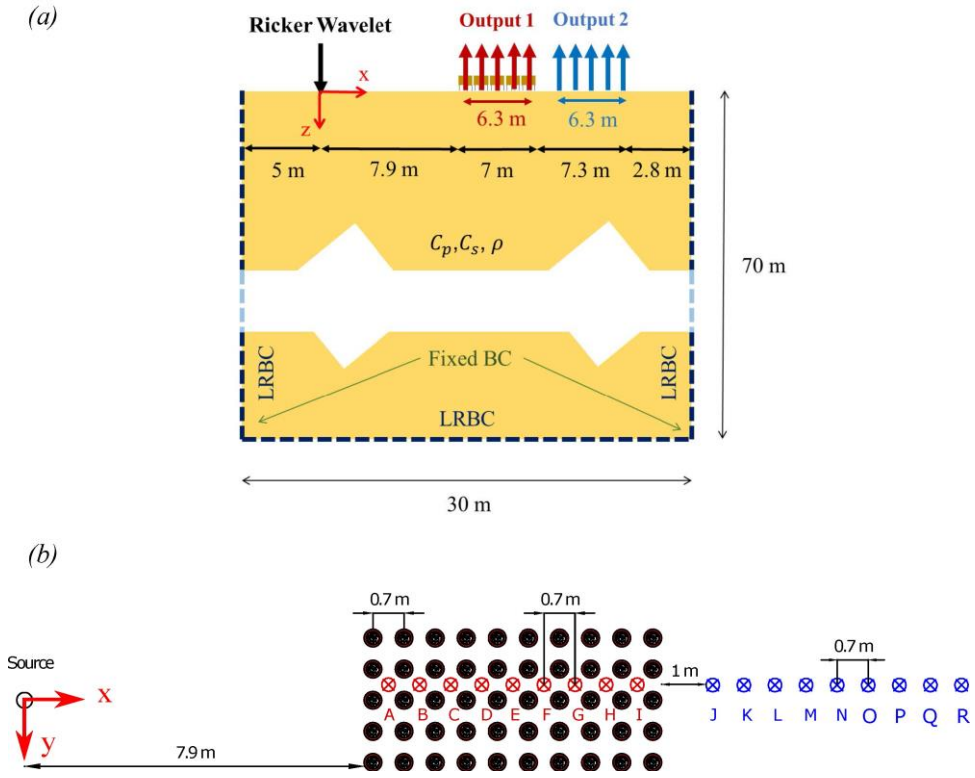

Figure 7. (a) Schematics of the full 2D FE model used in time history analyses. (b) The layout of on-field experimental test setup (instrumentation, source offsets, and barrier arrangement).

Frequency spectra of the averaged nodal displacements for RSM, DM, and MB configurations are calculated to quantify the attenuation performance of the barrier in terms of amplitude and frequency range, and the results are presented for the array output 1 and 2 in Fig. 8a and b, respectively. The addition of dead masses (DM) to the soil surface does not introduce a remarkable reduction in the surface wave spectrum. Comparison between the outputs extracted within (output 1) and outside (output 2) the DM array evidences minor changes in the spectrum ascribable to the dispersive effects in heterogeneous soils.

Conversely, the introduction of the resonators (MB) yields a considerable, although narrow, amplitude reduction around the resonant frequency of resonators f_r = 44 Hz, confirming the strong impedance mismatch between the resonant barrier and surface waves. Within the barrier, the amplitude reduction is accompanied by an amplitude peak (see Fig.8a) for frequencies approaching the barrier resonance, as a result of the surface confinement of the fundamental mode, displayed in Fig.6b. This peak disappears in the output recorded after the barrier (Fig.8b).

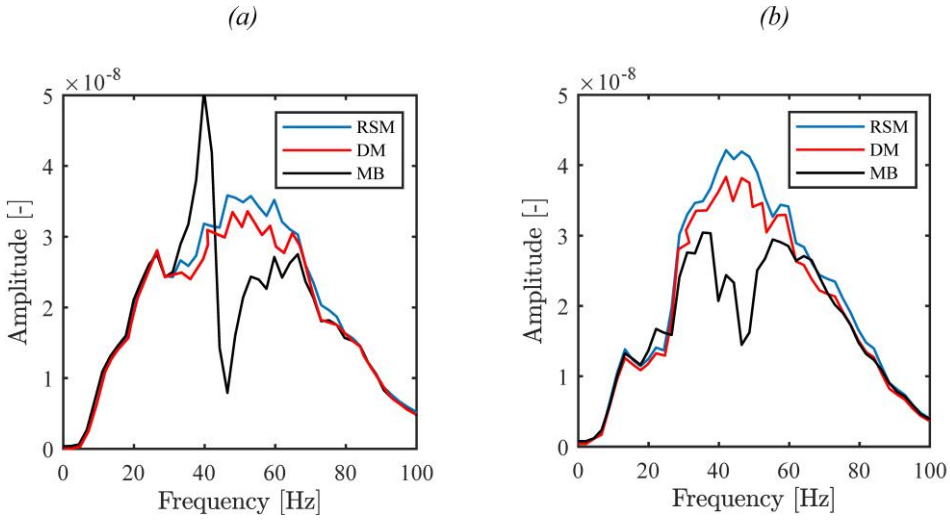

Figure 8. Frequency spectra of the vertical displacement fields generated by a Ricker wavelet with a central frequency of 50*Hz* obtained from the measurement (a) along the barrier (e.g., output 1), and (b) after the barrier (e.g., output2) for the RSM, DM, and MB configurations.

We perform a Two-Dimensional Fast Fourier Transform (2D FFT) to reconstruct the surface wave dispersion (frequency vs. wavenumber) from time responses calculated along with a line across the barrier (e.g., output 1). The 2D Fourier spectrum for the DM case is displayed in grayscale in Fig. 9a. The numerical dispersion obtained from the eigenfrequency analysis of the unit cell (see Fig. 4b) is superimposed to the figure.

Although the resolution in the wavenumber is limited due to the finite length of the measurement array, we can observe that the spectral amplitude of the surface displacement is located along the lowest branch predicted by the numerical dispersion curve.

The 2D Fourier spectrum of the surface waves travelling through the MB case is shown in Fig. 9b. Similar to the previous case, the surface modes calculated using the unit cell eigenfrequency analysis (Fig. 5b), are added to the figure. The results obtained via dispersion and time history analysis are in good agreement: the flat branch around the resonance frequency is well-predicted, and the lack of surface wave amplitude in the frequency region above the resonance confirms that higher-order modes do not contribute to the surface wavefield around the resonance frequency.

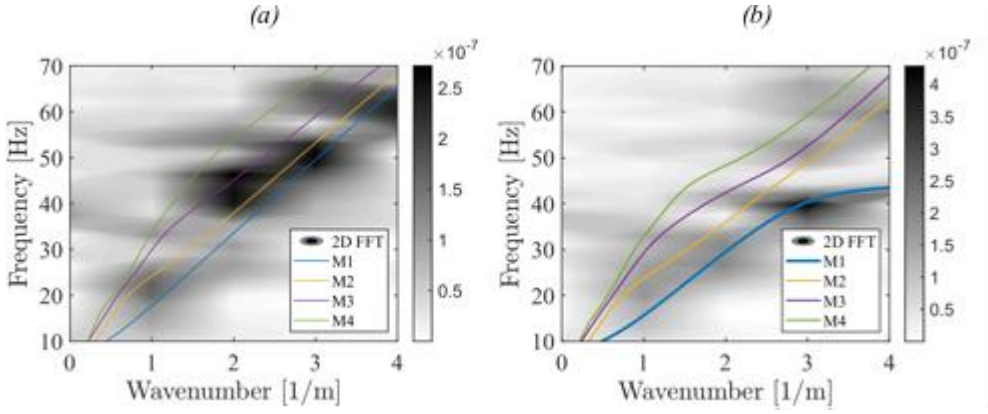

Figure 9. Dispersion spectra obtained from 2D FFTs of the time-domain surface displacements for the DM and MB cases (output 1). The dispersion curves predicted by the WFEM models in the Sec.3.1 are superimposed as continuous lines.

The vertical displacement fields of the RSM, and MB configurations, obtained from the time history analyses at the time instant t = 0.3 s, are presented in Fig. 10a and 10b, respectively. The wavefield map confirms a surface displacement reduction for

the MB case, ascribable to the dispersive nature of surface waves through the resonators and to the modified displacement profile, which gets confined below the surface.

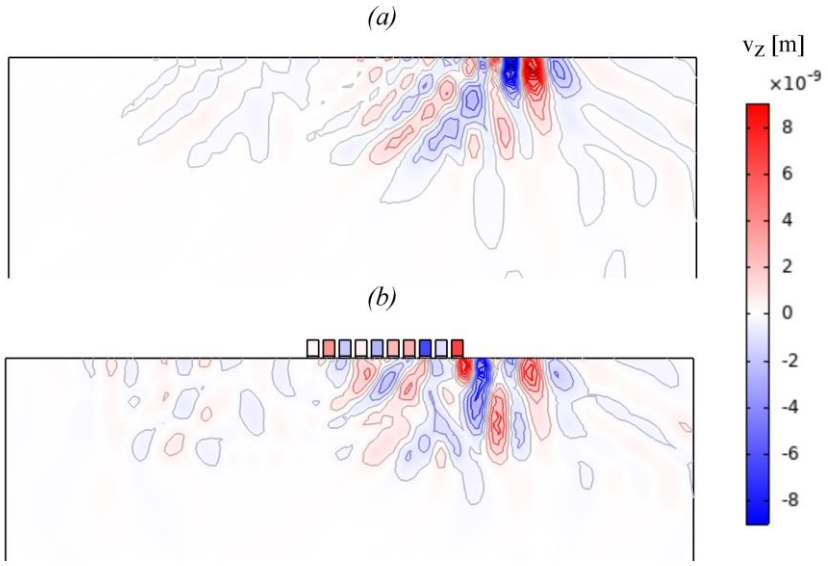

Figure 10. The vertical displacement field of (a) RSM, and (b) metabarrier (MB) configurations.

4. Graded resonant wave barrier

We leverage the tunable and modular design of the resonant wave barrier to build multiple-frequency barriers, e.g., barriers with graded resonant frequencies, for broadband attenuation purposes. The approach follows the idea of the "metawedge", originally presented in ref. (Colombi, Colquitt, et al., 2016) to discuss the dynamics of Rayleigh waves interacting with an array of elastic beams with increasing or decreasing frequencies.

The frequency-variable resonant barrier is formed by an array of equally distributed resonators with increasing or decreasing frequencies. The resonant frequencies of the resonators can be tailored by varying the mass (e.g., pouring different volumes of

sand into the barrels) or the vertical stiffness (e.g., modifying the number of springs) of the resonator. In the first case, by linearly increasing the mass of the resonators from 55 to 100 kg and keeping the number of springs constant (K_{tot} = 9869.6 kN/m), we reduce the natural frequency of resonators with a factor $1/\sqrt{d}$, where d is the resonator location along the array, as shown in Fig.11a. We can replicate this strategy to realize resonators with decreasing mass for a constant stiffness, to obtain a barrier with increasing frequency (Fig.11b). For both the configurations, the outputs are measured within (output 1) and after the barrier (output 2) through 9 sensors (see Fig.7a).

As first, we remind that the interaction of surface waves and a graded barrier with decreasing frequency (the so-called classical metawedge (Colombi, Colquitt, et al., 2016)) opens a wide bandgap in a homogeneous soil, where the surface waves are confined and back-reflected by the resonators. Here, for the considered heterogeneous soil, the behavior is similar. The wave motion is confined and amplified along the barrier, as evidenced by the wider amplitude peak shown in Fig.11c. After the barrier (see Fig.11e), a significant attenuation is observed as a result of the wave reflection.

On the contrary, for an increasing frequency barrier overlaying a homogeneous soil (i.e., the inverse metawedge (Colombi, Colquitt, et al., 2016)), the amplitude reduction is ascribable to the surface-to-shear wave conversion, with no displacement confinement along the barrier. In our heterogeneous soil configuration, although the surface-to-shear wave conversion is partially prevented by the higher-order surface modes, the behaviour of the barrier is similar. The surface wave energy is attenuated inside the barrier in a broader frequency range of approximately 40 − 70 Hz, and no

significant amplifications are observed (see Fig.11d). The amplitude in the attenuation frequency zone increases gradually as the resonant frequency increases. After the barrier (see Fig.11f), the attenuation performance remains similar, although a sharper peak attenuation is observed around 55 Hz.

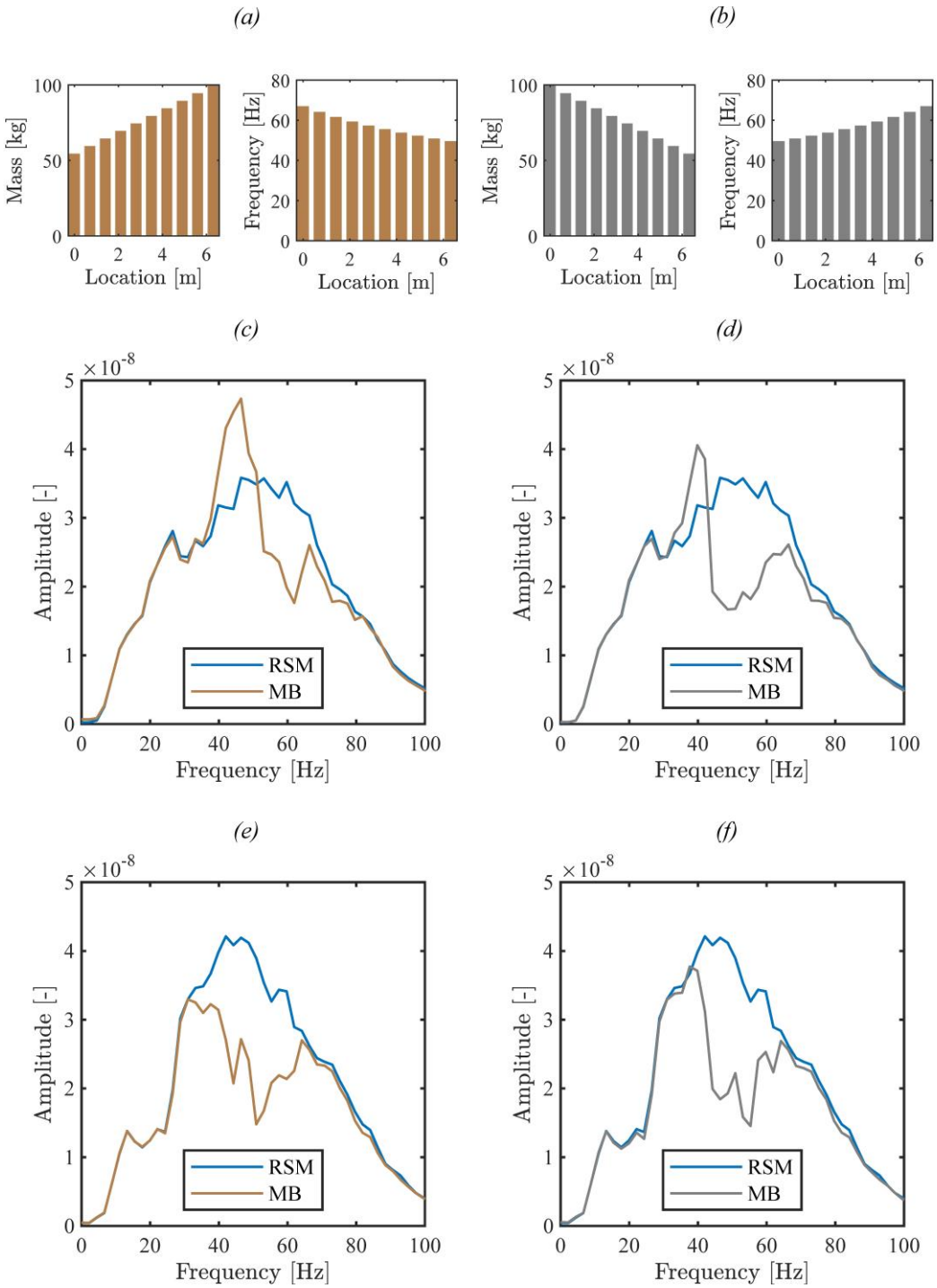

Figure 11. Mass distribution and the resonant frequency of the graded resonant barrier with increasing mass (a) and decreasing mass (b). Frequency spectra calculated along the graded barrier (output 1) with increasing mass (c) and decreasing mass (d) for a constant stiffness of the resonators. Frequency spectra after the graded barrier (output 2) with increasing mass (e) and decreasing mass (f) for a constant stiffness of the resonators (K_{tot} = 9869.6 *kN/m*).

Analogous results can be obtained by designing graded resonant wave barriers with constant mass (M = 100 kg) and varying stiffness of increasing and decreasing resonant frequencies, as shown in Fig.12a and b, respectively. For instance, we can build a barrier with an increasing number of springs per resonator, starting with a resonator with 4 springs and reaching up to 13 springs for the last resonator of the barrier. The increasing frequency barrier (with increasing stiffness) shows a dynamic behavior similar to the case with decreasing mass, as shown in Fig. 12c and e, for attenuation measurements along and after barrier, respectively. Conversely, by mirroring the distribution of the resonator along the array, so to obtain a barrier with decreasing frequency, a wider range of frequency where surface waves are confined and amplified within (Fig. 12d) and after the barrier (Fig. 12e) is obtained. The broader frequency range covered by the barrier allows us to obtain a wider frequency range of attenuation.

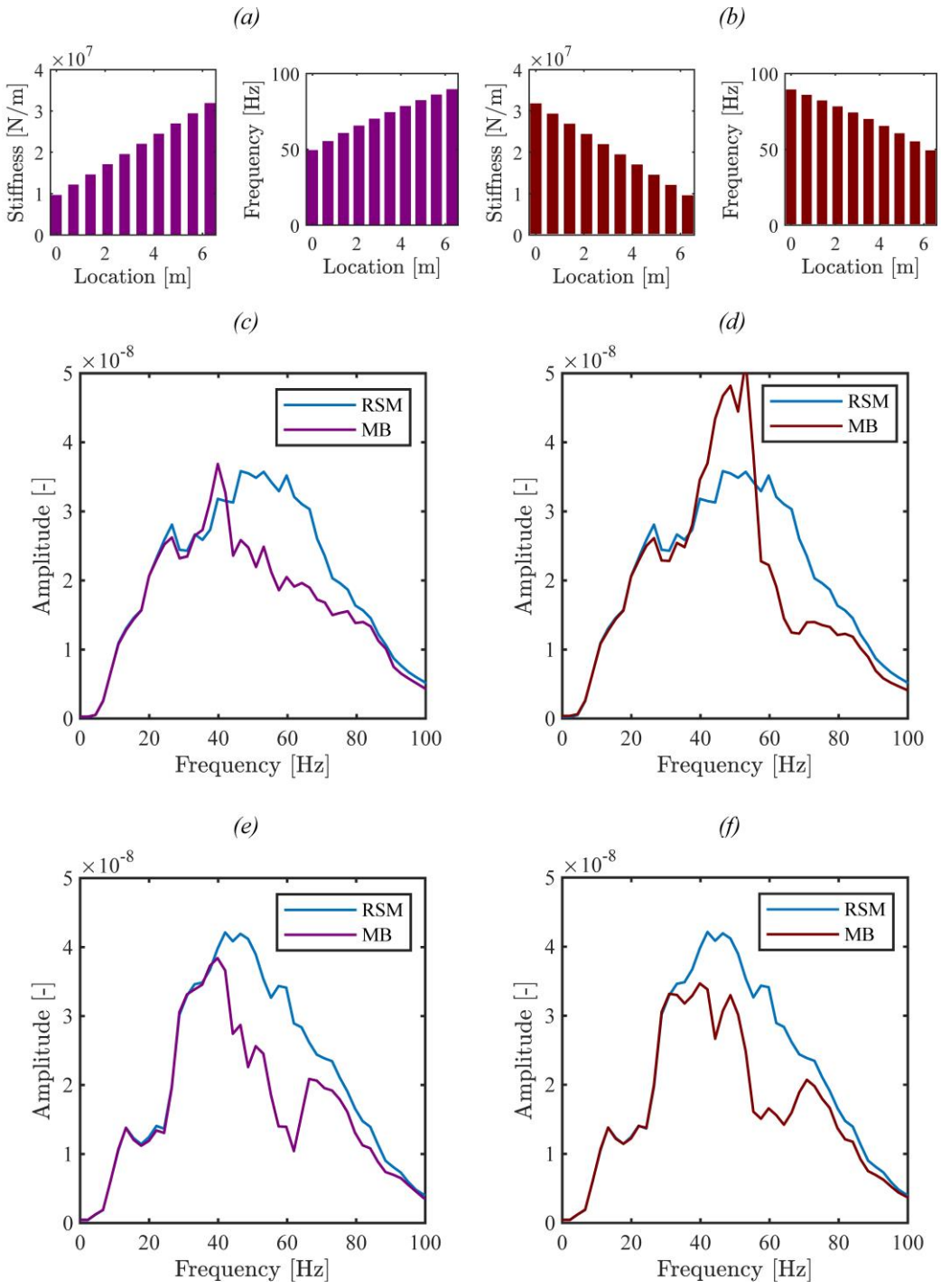

Figure 12. Stiffness and the resonant frequency of the graded resonant barrier with increasing stiffness (a) and decreasing stiffness (b). Frequency spectra calculated along the graded barrier (output 1) with increasing vertical stiffness (c) and decreasing vertical stiffness (d) for a constant mass of the resonators. Frequency spectra

calculated after the graded barrier (output 2) with increasing vertical stiffness (e) and decreasing vertical stiffness (f) for a constant mass of the resonators (M = 100 kg).

5. Conclusions

The resonant wave barrier is a passive isolation device consisting of an array of mechanical oscillators (mass-springs) placed over the soil surface in the vicinity of the structure or infrastructure to protect. In this study, the wave attenuation performance of a medium-size scale resonant barrier placed atop of a heterogeneous soil is assessed numerically, to provide the guideline of an experimental campaign aimed at assessing the efficiency of the metabarrier on the field.

The resonant wave barrier exploits the local resonances of resonators to damp the propagation of seismic surface waves at the frequency ranges close to the characteristic resonant frequency of the oscillators. A finite-length barrier is modeled to measure the attenuation of surface waves travelling within and after the barrier. A significant surface wave attenuation is observed in a narrow frequency band around the resonant frequency of the barrier. Resonators with varying natural frequencies, increasing or decreasing along the array, are employed to achieve broadband attenuation of surface waves. The operating frequencies of the frequency-variable barriers are tuned by changing the stiffness (number of springs) or mass of the resonators.

A companion numerical model is developed for the “dead mass” configuration, e.g., an array of the masses directly placed over the soil surface. The addition of a masses on the soil surface yields a minimal attenuation of the surface waves, confirming that

the attenuation in the wave barrier is ascribable to the effect of the resonant dynamics.

We believe that the numerical framework and the outcomes of this research can provide a better understanding of the dynamics of locally resonant devices. In particular, the promising results in terms of surface ground motion attenuation obtained via time-domain analysis, developed for both single frequency and graded barriers, support the realization of on-field experiments in the Euroseistest area.

Disclosure statement

The authors have no conflicts of interest to declare.

Funding

We acknowledge support by the project "Seismology and Earthquake Engineering Research Infrastructure Alliance for Europe (SERA)". This project has received funding from the European Union's Horizon 2020 research and innovation programme under grant agreement No.730900.

References

Achaoui, Y., Antonakakis, T., Brûlé, S., Craster, R. V., Enoch, S., & Guenneau, S. (2017). Clamped seismic metamaterials: ultra-low frequency stop bands. *New Journal of Physics*, *19*(6), 063022.

Antoniadis, I. A., Kanarachos, S. A., Gryllias, K., & Sapountzakis, I. E. (2018). Kdamping: A stiffness based vibration absorption concept. *Journal of Vibration and Control*, *24*(3), 588-606.

Bao, J., Shi, Z., & Xiang, H. (2011). Dynamic responses of a structure with periodic foundations. *Journal of Engineering Mechanics*, *138*(7), 761–769.

Basone, F., Wenzel, M., Bursi, O. S., & Fossetti, M. (2019). Finite locally resonant metafoundations for the seismic protection of fuel storage tanks. *Earthquake Engineering & Structural Dynamics*, *48*(2), 232-252.

Brûlé, S., Javelaud, E. H., Enoch, S., & Guenneau, S. (2014). Experiments on seismic metamaterials: Molding surface waves. *Phys. Rev. Lett.*, *112*, 133901.

Cheng, Z., & Shi, Z. (2013). Novel composite periodic structures with attenuation zones. *Engineering Structures*, *56*, 1271 - 1282.

Cheng, Z., & Shi, Z. (2018). Composite periodic foundation and its application for seismic isolation. *Earthquake Engineering & Structural Dynamics*, *47*(4), 925-944.

Cheng, Z., Shi, Z., Palermo, A., Xiang, H., Guo, W., & Marzani, A. (2020). Seismic vibrations attenuation via damped layered periodic foundations. *Engineering Structures*, *211*, 110427.

Colombi, A., Colquitt, D. J., Roux, P. P., Guenneau, S., & Craster, R. V. (2016). A seismic metamaterial: The resonant metawedge. *Scientific reports*, *6*, 27717.

Colombi, A., Guenneau, S., Roux, P., & Craster, R. V. (2016). Transformation seismology: composite soil lenses for steering surface elastic rayleigh waves. *Scientific Reports*, *6*, 25320.

Colombi, A., Roux, P., Guenneau, S., Gueguen, P., & Craster, R. V. (2016). Forests as a natural seismic metamaterial: Rayleigh wave bandgaps induced by local resonances. *Scientific Reports*, *6*, 19238.

Colquitt, D., Colombi, A., Craster, R., Roux, P., & Guenneau, S. (2017). Seismic metasurfaces: Sub-wavelength resonators and rayleigh wave interaction. *Journal of the Mechanics and Physics of Solids*, *99*, 379 - 393.

Dertimanis, V. K., Antoniadis, I. A., & Chatzi, E. N. (2016). Feasibility analysis on the attenuation of strong ground motions using finite periodic lattices of mass-in-mass barriers. *Journal of Engineering Mechanics*, *142*(9), 04016060.

Furinghetti, M., & Pavese, A. (2017). Equivalent uniaxial accelerogram for css-based isolation systems assessment under two-components seismic events. *Mechanics Based Design of Structures and Machines*, *45*(3), 282-295.

Kadic, M., Bückmann, T., Schittny, R., & Wegener, M. (2013). Metamaterials beyond electromagnetism. *Reports on Progress in Physics*, *76*(12), 126501. K.F. Graff. (1975). *Wave motion in elastic solids*. Dover.

Krödel, S., Thomé, N., & Daraio, C. (2015). Wide band-gap seismic metastructures. *Extreme Mechanics Letters*, *4*, 111 - 117.

Mace, B. R., & Manconi, E. (2008). Modelling wave propagation in two-dimensional structures using finite element analysis. *Journal of Sound and Vibration*, *318*(4), 884–902.

Maurel, A., Marigo, J.-J., Pham, K., & Guenneau, S. (2018). Conversion of love waves in a forest of trees. *Phys. Rev. B*, *98*, 134311.

Mazza, F., & Sisinno, S. (2017). Nonlinear dynamic behavior of base-isolated buildings with the friction pendulum system subjected to near-fault earthquakes. *Mechanics Based Design of Structures and Machines*, *45*(3), 331-344.

Miniaci, M., Krushynska, A., Bosia, F., & Pugno, N. M. (2016). Large scale mechanical metamaterials as seismic shields. *New Journal of Physics*, *18*(8), 083041.

P. A. Deymier. (2013). *Acoustic metamaterials and phononic crystals*. Springer.

Palermo, A., Krödel, S., Marzani, A., & Daraio, C. (2016). Engineered metabarrier as shield from seismic surface waves. *Scientific Reports*, *6*, 39356.

Palermo, A., Krödel, S., Matlack, K. H., Zaccherini, R., Dertimanis, V. K., Chatzi, E. N., ... Daraio, C. (2018). Hybridization of guided surface acoustic modes in unconsolidated granular media by a resonant metasurface. *Phys. Rev. Applied*, *9*, 054026.

Palermo, A., Zeighami, F., Vratsikidis, A., Cheng, Z., Pitilakis, D., & Marzani, A. (2019). Design of a medium-scale test for the assessment of a resonant seismic barrier within the reward project. *DSTA-2019 Conference Books: Theoretical Approaches in Non-linear Dynamical Systems, 1, 393-405*.

Pendry, J. B., Holden, A. J., Stewart, W. J., & Youngs, I. (1996). Extremely low frequency plasmons in metallic mesostructures. *Phys. Rev. Lett.*, *76*, 4773–4776.

Pitilakis, D., Dietz, M., Wood, D. M., Clouteau, D., & Modaressi, A. (2008). Numerical simulation of dynamic soil–structure interaction in shaking table testing. *Soil Dynamics and Earthquake Engineering*, *28*(6), 453 - 467.

Pitilakis, D., Rovithis, E., Anastasiadis, A., Vratsikidis, A., & Manakou, M. (2018). Field evidence of ssi from full-scale structure testing. *Soil Dynamics and Earthquake Engineering*, *112*, 89 - 106.

Pitilakis, K., Raptakis, D., Lontzetidis, K., Tika-Vassilikou, T., & Jongmans, D. (1999). Geotechnical and geophysical description of euro-seistest, using field, laboratory tests and moderate strong motion recordings. *Journal of Earthquake Engineering*, *3*(3), 381-409.

Pu, X., & Shi, Z. (2018). Surface-wave attenuation by periodic pile barriers in layered soils. *Construction and Building Materials*, *180*, 177 - 187.

Raptakis, D., Chavez-Gracia, F., Makra, K., & Pitilakis, K. (2000). Site effects at euroseistest—I. Determination of the valley structure and confrontation of observations with 1D analysis. *Soil Dynamics and Earthquake Engineering*, *19*(1), 1 - 22.

Shi, Z., Cheng, Z., & Xiang, H. (2014). Seismic isolation foundations with effective attenuation zones. *Soil Dynamics and Earthquake Engineering*, *57*, 143–151.

Sun, F., Xiao, L., & Bursi, O. S. (2020). Quantification of seismic mitigation performance of periodic foundations with soil-structure interaction. *Soil Dynamics and Earthquake Engineering*, *132*, 106089.

Yan, Y., Laskar, A., Cheng, Z., Menq, F., Tang, Y., Mo, Y. L., & Shi, Z. (2014). Seismic isolation of two dimensional periodic foundations. *Journal of Applied Physics*, *116*(4), 044908.

Zaccherini, R., Colombi, A., Palermo, A., Dertimanis, V. K., Marzani, A., Thomsen, H. R., ... Chatzi, E. N. (2020). Locally resonant metasurfaces for shear waves in granular media. *Phys. Rev. Applied*, *13*, 034055.

Zeighami, F., Palermo, A., & Marzani, A. (2019). Inertial amplified resonators for tunable metasurfaces. *Meccanica*, *54*, 2053-2065.